Ultralight Heterostructured Aerogels of $ZnO/ZnFe_2O_4/Fe_3O_4/RGO/MWCNT$ for Ultra-Broadband Microwave Absorption

Farnaz Jamadi[1,2], Jamileh Seyed-Yazdi[1,*], Seyyed Jalal Seyyedyazdi[3]

[1]Department of Physics, Faculty of Science, Vali-e-Asr University of Rafsanjan, Rafsanjan, Iran.

[2]Department of Physics, Sirjan University of Technology, Sirjan, Iran.

[3]Department of Computer Science, Vali-e-Asr University of Rafsanjan, Rafsanjan, Iran.

*Corresponding author: j.seyedyazdi@gmail.com

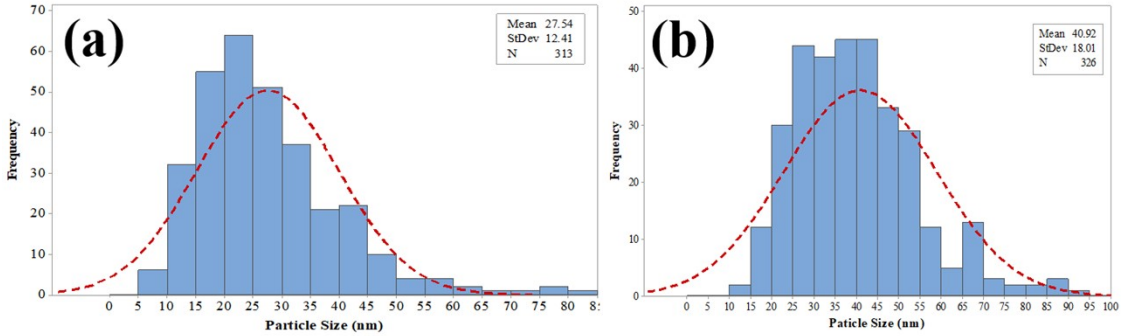

Fig. SI-1. Particle size distributions which demonstrate nearly uniform dispersion of Fe_3O_4 on the RGO substrate for S_2 (a), and S_3 (b).

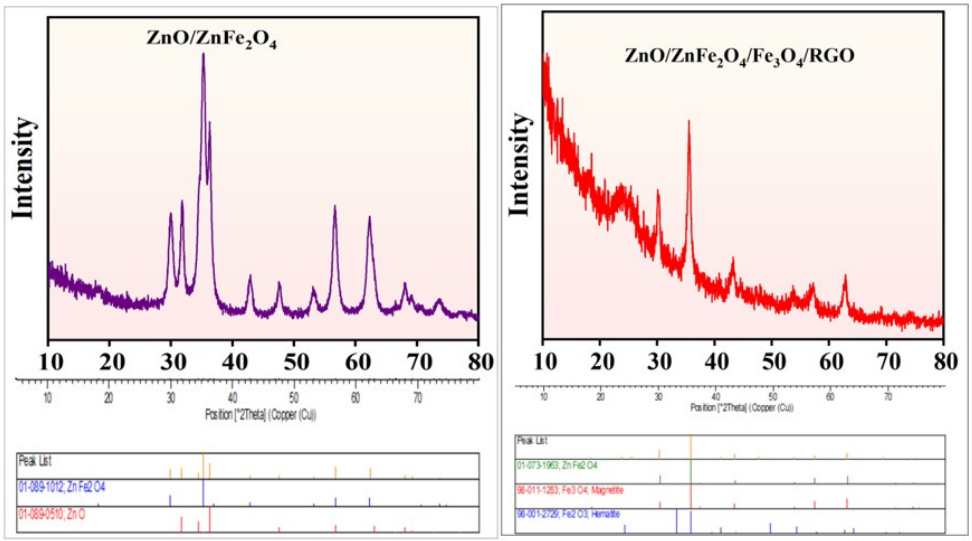

Fig. SI-2. XRD patterns of $ZnO/ZnFe_2O_4$ (S_1), $ZnO/ZnFe_2O_4/Fe_3O_4/RGO$ (S_2) samples.

The magnetic response of ferromagnetic materials in high external magnetic fields can be effectively described by the phenomenological law of approach to saturation, commonly expressed as a series expansion, Eq. (1) [s1]:

$$M = M_s\left(1 - \frac{A}{H} - \frac{B}{H^2}\right) + \chi H \qquad (1)$$

Where M_s is the saturation magnetization, and A, B, and χ are constants connected to specific physical phenomena. The parameter A accounts for effects arising from inclusions and micro-stress within the material, B correlates with the magneto-crystalline anisotropy, and the term χH represents the forced magnetization induced by high magnetic fields, which becomes particularly relevant at elevated temperatures [s2]. According to established guidelines (Cullity and Graham) [s3], the term involving A/H, associated with inclusions and micro-stress effects, is typically significant only over limited field ranges and is often regarded as negligible in high-field regimes [s1]. Likewise, the contribution of the χH term is considered negligible because, in high magnetic fields, plotting M against $1/H^2$ yields a linear fit with high accuracy. This approach enables the extraction of the saturation magnetization M_s from the intercepts of the linear fits in the M versus $1/H^2$ plots, as demonstrated in Fig. SI-3. Applying Eq. (1), the saturation magnetization values for samples S_1, S_2, and S_3 were determined to be 2.7 emu/g, 13.6 emu/g, and 7.7 emu/g, respectively.

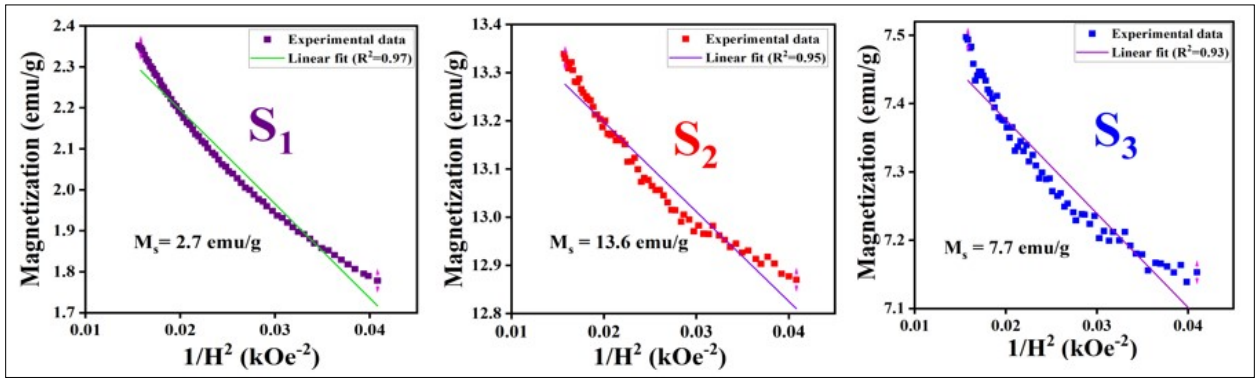

Fig. SI-3. Magnetization versus $1/H^2$ for $ZnO/ZnFe_2O_4$ (S_1), $ZnO/ZnFe_2O_4/Fe_3O_4/RGO$ (S_2), and $ZnO/ZnFe_2O_4/Fe_3O_4/RGO/MWCNT$ (S_3), samples.

According to the experimental section, sample S2 contains 0.2 g RGO and is measured at 20 wt% filler in paraffin, and sample S3 contains the same 0.2 g RGO plus 0.013 g MWCNTs, but is measured at only 10 wt% filler in paraffin. Therefore, the lower dielectric conductivity of S3 (depicted in Fig. SI-4) is a direct consequence of the reduced overall filler concentration, not an inherent property of MWCNTs. When comparing samples with identical filler loadings (which we are currently preparing for a follow-up study), the inclusion of MWCNTs consistently enhances conductivity and loss.

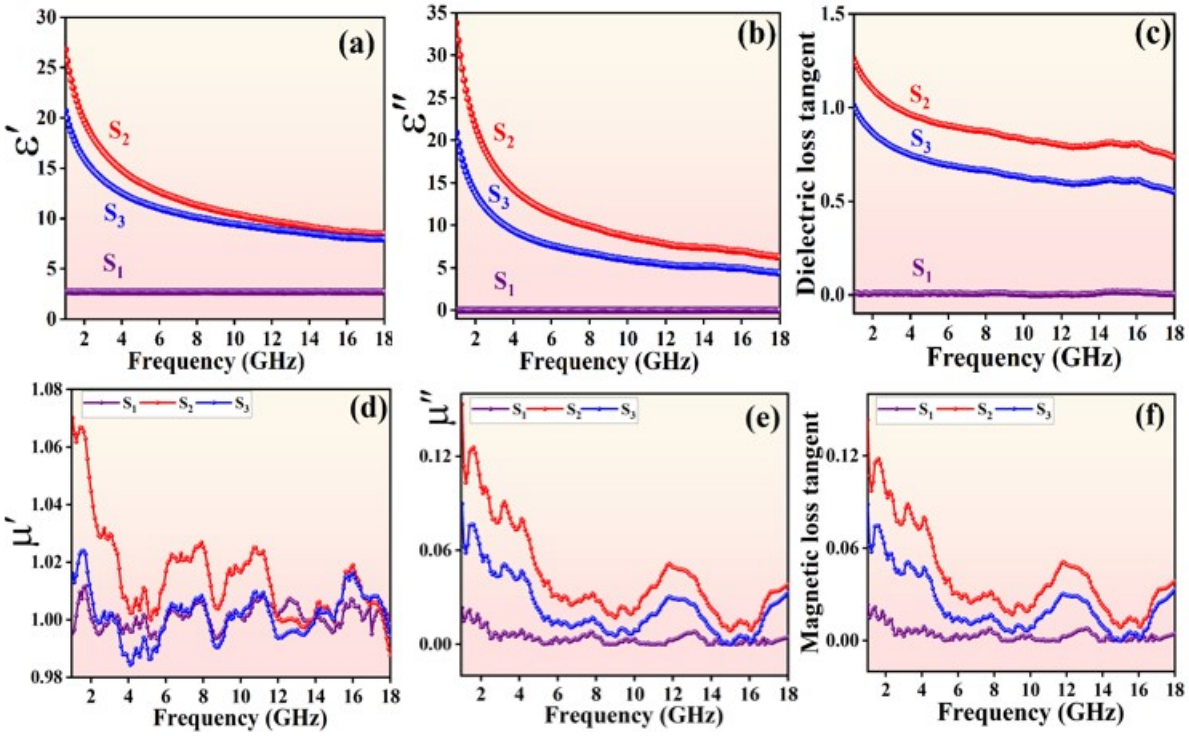

Fig. SI-4. (a,b) real part (ε′), and imaginary part (ε″) of complex permittivity, (c) dielectric loss tangent, (d,e) real part (μ′) and imaginary part (μ″) of complex permeability, (f) magnetic loss tangent, respectively for ZnO/$ZnFe_2O_4$ (S_1), ZnO/$ZnFe_2O_4$/Fe_3O_4/RGO (S_2), and ZnO/$ZnFe_2O_4$/Fe_3O_4/RGO/MWCNT (S_3), samples.

A direct comparison of RL and EAB values is presented for samples S_1, S_2, and S_3 in Fig. SI-5. The bar charts confirm that the S_3 aerogel achieves both the lowest RL and the widest EAB, representing the most effective and broadband absorber in this study.

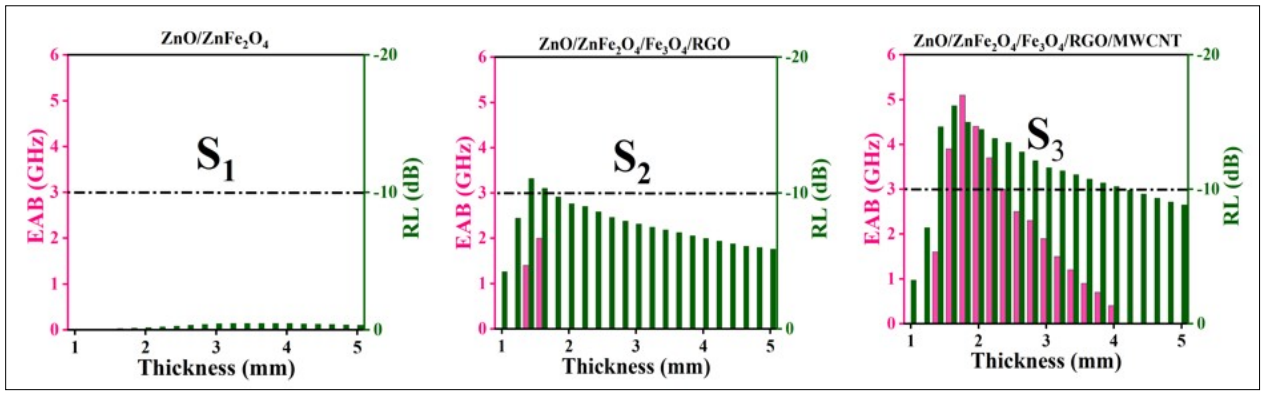

Fig. SI-5. EAB and reflection loss column charts for $ZnO/ZnFe_2O_4$ (S_1), $ZnO/ZnFe_2O_4/Fe_3O_4/RGO$ (S_2), and $ZnO/ZnFe_2O_4/Fe_3O_4/RGO/MWCNT$ (S_3), samples.

The two-dimensional (2D) and counter diagrams illustrating the coefficient of input impedance matching (M_z), are comprehensively presented across all samples in Fig. SI-6. As illustrated, sample S_3 exhibits favorable M_z values, indicating efficient impedance matching and superior electromagnetic wave absorption compared with samples S_1 and S_2.

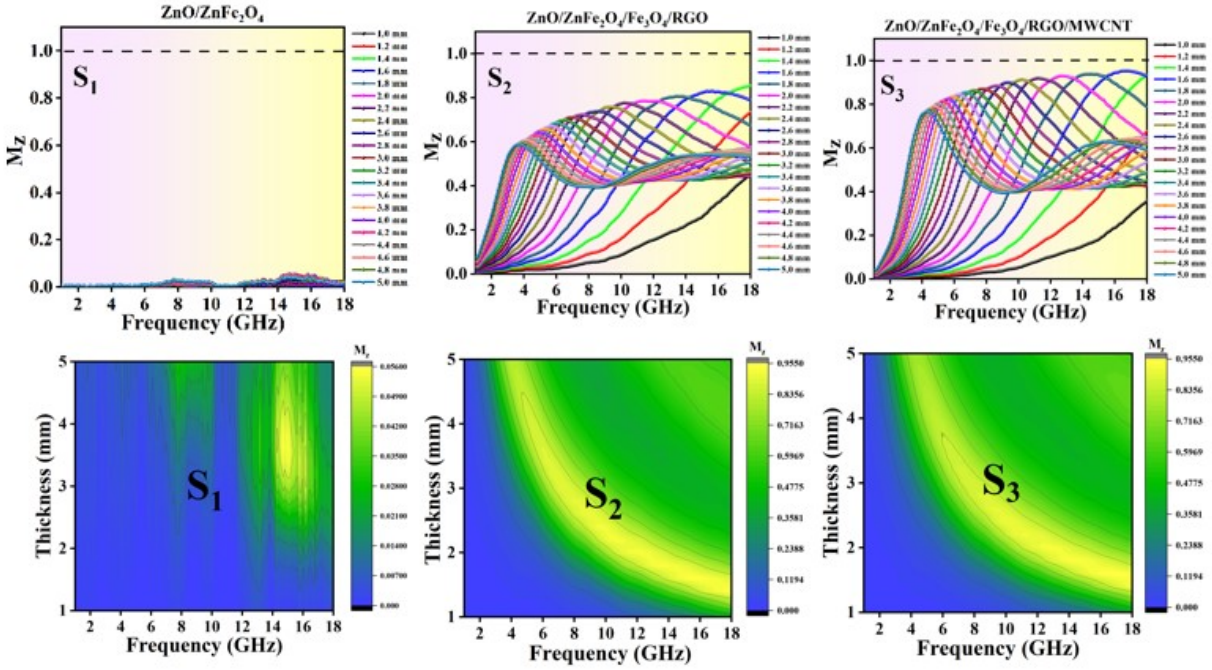

Fig. SI-6. 2D (first row) and contour (second row) diagrams of input impedance matching coefficient for $ZnO/ZnFe_2O_4$ (S_1), $ZnO/ZnFe_2O_4/Fe_3O_4/RGO$ (S_2), and $ZnO/ZnFe_2O_4/Fe_3O_4/RGO/MWCNT$ (S_3) samples.

The correlation between the real (ε′) and imaginary (ε″) parts of permittivity is further analyzed using Eq. (2), providing deeper insights into the polarization-relaxation processes.

$$\varepsilon' = \frac{1}{2\pi\tau}\frac{\varepsilon''}{f} + \varepsilon_\infty \qquad (2)$$

When dielectric loss is dominated by a polarization-relaxation mechanism, the relaxation time (τ) can be determined by examining the slope of the linear relationship between ε' and ε''/f, as depicted in Fig. SI-7. Variations in this slope reflect the dynamics of dipole orientation. Fitting three linear

segments reveals multiple relaxation processes influencing dielectric loss and microwave absorption [s4]. As seen in Fig. SI-7, the relaxation time of the S_2 sample is longer than that of the S_3 sample.

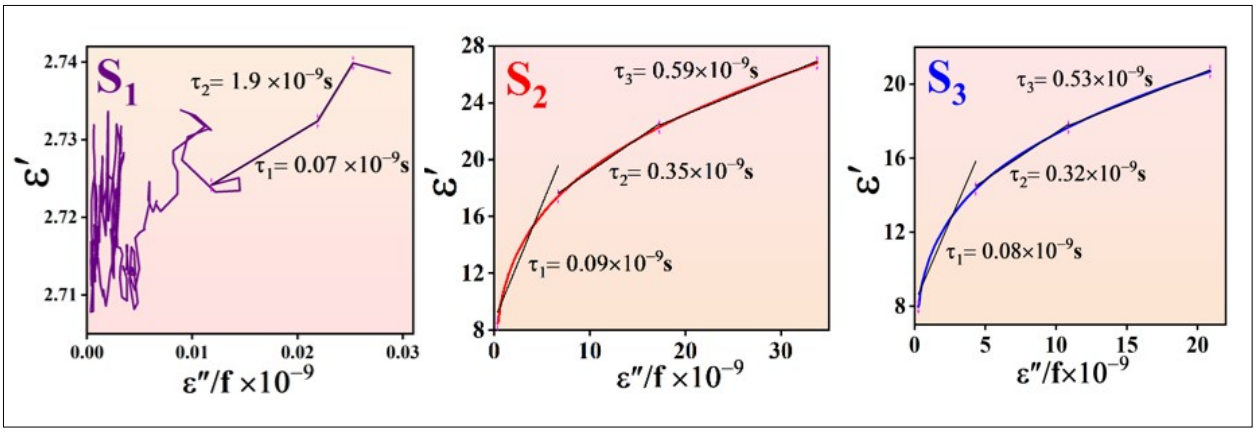

Fig. SI-7. The ε′ versus ε″/f diagrams for $ZnO/ZnFe_2O_4$ (S_1), $ZnO/ZnFe_2O_4/Fe_3O_4/RGO$ (S_2), and $ZnO/ZnFe_2O_4/Fe_3O_4/RGO/MWCNT$ (S_3), samples.

References

[s1] Suliga, M. and K. Chwastek, Effect of stress in drawn wires on magnetization curves in the saturation region. Acta Physica Polonica A, 2019. **135**(2): p. 243-245.

[s2] Awawdeh, M., I. Bsoul, and S. Mahmood, Magnetic properties and Mössbauer spectroscopy on Ga, Al, and Cr substituted hexaferrites. Journal of Alloys and Compounds, 2014. **585**: p. 465-473.

[s3] Cullity, B.D. and C.D. Graham, Introduction to magnetic materials. 2011: John Wiley & Sons.

[s4] Zhou, X., et al., Electromagnetic wave absorption performance of $NiCo_2X_4$ (X= O, S, Se, Te) spinel structures. Chemical Engineering Journal, 2021. **420**: p. 129907.